Tetrahedron 66 (2010) 7954–7960

Contents lists available at ScienceDirect

Tetrahedron

journal homepage: www.elsevier.com/locate/tet

Heterocyclic quinol-type fluorophores. Part 9: Effect of forming a continuous intermolecular hydrogen bonding chain between fluorophores on the solid-state fluorescence properties☆

Yousuke Ooyama *, Saori Nabeshima, Toshiki Mamura, Haruka Egawa Ooyama, Katsuhira Yoshida *

Department of Material Science, Faculty of Science, Kochi University, Akebono-cho, Kochi 780-8520, Japan

ARTICLE INFO

Article history:
Received 23 July 2010
Received in revised form 7 August 2010
Accepted 10 August 2010
Available online 14 August 2010

ABSTRACT

Three heterocyclic quinol-type fluorophores with benzo[*c*]carbazol-6-one skeleton or benzo[*b*]naphtho[1,2-*d*]furan-6-one skeleton, 9-dibutylamino-5-hydroxy-5-phenyl-5,7-dihydro-benzo[*c*]carbazol-6-one (**5a**), 7-butyl-9-dibutylamino-5-hydroxy-5-phenyl-5,7-dihydro-benzo[*c*]carbazol-6-one (**5b**) and 9-dibutylamino-5-hydroxy-5-phenyl-5*H*-benzo[*b*]naphtho[1,2-*d*]furan-6-one (**6c**) have been synthesized and their photophysical properties have been investigated in solution and in the solid state. The fluorescence quantum yield (Φ) increases in the order of **5b** (0.35)<**5a** (0.41)<**6c** (0.74) in 1,4-dioxane. On the other hand, the Φ value in the solid state increases in the order of **5a**<<**6C** (0.03)<**5b** (0.07), which are much smaller than those in 1,4-dioxane. To elucidate the effects of molecular and crystal structures on the solid-state fluorescence properties, we have performed the semi-empirical molecular orbital calculations (AM1 and INDO/S) and X-ray crystallographic analysis. It was found that the formation of a continuous intermolecular hydrogen bonding between adjacent fluorophores is observed in the crystal of **5a**, which is considered to cause a drastic fluorescence quenching in the solid state.

1. Introduction

Solid-state organic fluorescent dyes have received considerable attention because of not only for fundamental use in the research of solid-state photochemistry,[1] but also for practical use in the organic light emitting diode (OLED)[2] and optical sensor[3] fields. Although there are many dyes exhibiting strong fluorescence in solution, the number of fluorescent dyes exhibiting intense fluorescence in the solid state is relatively limited because most organic fluorophores undergo fluorescence quenching in aggregation state. The solid-state fluorescence properties are closely associated with the molecular packing structure, and many researches have been conducted on the correlation between the solid-state fluorescence properties and the molecular packing structures on the basis of the X-ray crystal structures. It has been revealed that strong intermolecular interactions, such as π–π interaction and intermolecular hydrogen bonding between neighboring fluorophores are principal factors of fluorescence quenching in the solid state.[1d,3,4] Consequently, the key point in designing the new strong solid-state emissive fluorophores is to reduce the intermolecular interactions between fluorophores leading to fluorescence quenching in molecular aggregation states. For example, the introduction of bulky substituents to the original fluorophores and the construction of a non-planar structure with sterical hindered substituents are known to be very useful methods for solving the problem of fluorescence quenching by aggregation.[5,6] Akkaya et al. have recently reported solid-state emissive BODIPY dyes with bulky substituents as spacers; introduction of bulky *tert*-butyl substituents on the *meso*-phenyl groups result in more spaced packing in the solid-state, leading to highly luminescent powders and films.[7] On the other hand, Tang et al. have discovered a very interesting solid-state fluorescence system that a series of silole molecules were found to be non-luminescent in the solution state but emissive in the aggregated state. They coined the term 'aggregation-induced emission (AIE)' for this novel phenomenon and identified restriction of intramolecular rotation leading to non-radiative decay in the aggregates as a main cause for the AIE effect.[8] Thus, in order to control perfectly the solid-state fluorescence properties of organic fluorophores, it is necessary to obtain further useful information about the effect of molecular and crystal structures on the solid-state fluorescence properties.

In our previous study, we have reported the synthesis of novel heterocyclic quinols, 5-hydroxy-5-substituent-benzo[*b*]naphtho[1,2-*d*]furan-6-one fluorophores (**6a**–**c**) with substituents (R=Me,

☆ For part 8 in the series, see Ref. 6e.

* Corresponding authors. Tel.: +81 88 844 8296; fax: +81 88 844 8359.; e-mail addresses: yooyama@hiroshima-u.ac.jp (Y. Ooyama), kyoshida@cc.kochi-u.ac.jp (K. Yoshida).

0040-4020/$ – see front matter © 2010 Elsevier Ltd. All rights reserved.
doi:10.1016/j.tet.2010.08.026

Bu and Ph) of non-conjugated linkage to the chromophores and their absorption and fluorescence properties in solution and in the solid state (Scheme 1).[6a] Dramatic substituent effects on the solid-state photophysical properties were observed, which has been elucidated by means of the X-ray crystallographic analysis. It was confirmed that the formation of intermolecular π–π interactions between the fluorophores in molecular aggregation states is dependent on the substituents, leading to the differences of the solid-state fluorescence properties among fluorophores (**6a**–**c**).

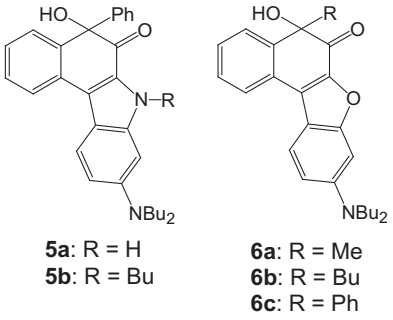

Scheme 1. Heterocyclic quinol-type fluorophores **5a**, **5b**, and **6a**–**c**.

In this work, to obtain further information about the effect of molecular and crystal structures in aggregation state on the solid-state fluorescence properties, we have newly synthesized heterocyclic quinol-type fluorophores, 9-dibutylamino-5-hydroxy-5-phenyl-5,7-dihydro-benzo[*c*]carbazol-6-one (**5a**) and 7-butyl-9-dibutylamino-5-hydroxy-5-phenyl-5,7-dihydro-benzo[*c*]carbazol-6-one (**5b**) (Scheme 1), and their photophysical properties along with **6c** have been investigated in solution and in the solid state. Considerable differences in the photophysical properties among the fluorophores **5a**, **5b**, and **6c** were observed both in solution and in the solid state. On the basis of the results of the semi-empirical molecular orbital calculations (AM1 and INDO/S) and the X-ray crystal structures, the relations between the solid-state fluorescence properties and the molecular and crystal structures are discussed.

2. Result and discussion

2.1. Synthesis

We first prepared the starting heterocyclic quinones **1** and **3** as shown in Scheme 2. The reaction of sodium 1,2-naphthoquinone-4-sulfonate with *m*-amino-*N*,*N*-dibutylaniline in acetic acid in the presence of $Ni(OCOCH_3)_2$ gave 4-arylated-benzo[*c*]carbazole-5,6-dione (**1**) and 4-aminated-1,2-naphthoquinone (**2**) in 5% and 35% yields, respectively. On the other hand, the reaction of sodium 1,2-naphthoquinone-4-sulfonate with *m*-butylamino-*N*,*N*-dibutylaniline in DMF in the presence of $CuCl_2$ gave two structural isomers of 4-arylated-*N*-butylbenzo[*c*]carbazole-5,6-dione (**3**) and 4-aminated-benzo[*a*]carbazole-5,6-dione (**4**) in 39% and 13% yields, respectively. In both reactions, the formation of a metal chelate complex between the *o*-quinone carbonyl groups and the metal ion probably facilitates the nucleophilic desulpho-amination or the nucleophilic desulpho-arylation at the 4-position, and the following intramolecular cyclization occurs to produce *o*-quinones with benzo[*a*]carbazole or benzo[*c*]carbazole skeleton, **1**, **3**, and **4**. Interestingly, in both reactions, the 4-arylation is in competition with the 4-amination. The former reaction gives preference to the 4-amination over the 4-arylation, because the nucleophilicity of amino group in *m*-amino-*N*,*N*-dibutylaniline is higher than that of the *ortho* position of the aniline. Thus, the former reaction afforded preferentially the 4-aminated-1,2-naphthoquinone (**2**). On the other hand, the latter reaction gives preference to the 4-arylation over the 4-amination, because the sterically hindered *N*-butylamino group in *m*-butylamino-*N*,*N*-dibutylaniline makes it difficult for the nucleophilic desulpho-amination. Thus, the latter reaction afforded preferentially the 4-arylated-*N*-butylbenzo[*c*]carbazole-5,6-dione (**3**).

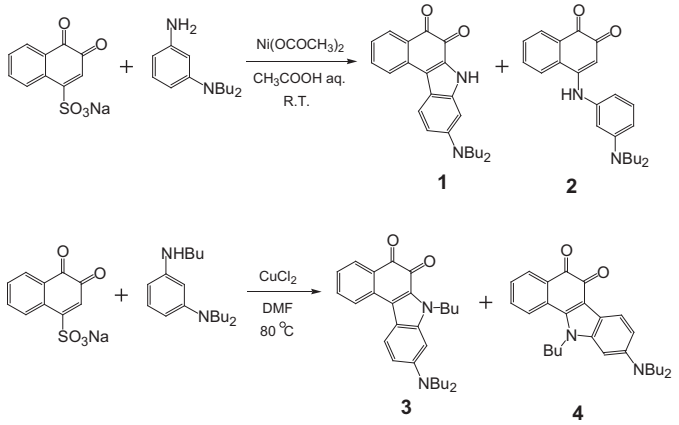

Scheme 2. Synthesis of *o*-quinones **1**–**4**.

As shown in Scheme 3, the heterocyclic quinols **5a** and **5b** were obtained in 21% and 12% yields by the reaction of quinones **1** and **3** with phenyllithium (PhLi) at −108 °C, respectively. It is known that the addition of organometallic reagents to quinones gives not only quinols but also hydroquinone as a by-product: both the 1,2-addition and the reduction of the quinoid skeleton by organometallic reagents proceed competitively.[9] In our case, the corresponding hydroquinone produced in situ was easily reoxidized by atmospheric oxygen during work-up of the reaction mixture, resulting in recovery of the starting quinine (40% for **1** and 32% for **3**). For the quinones **1** and **3**, PhLi reagent preferentially attack the 5-carbonyl carbon than the 6-carbonyl in spite of the similar steric reactivity of the two carbonyls. The conjugated linkage of the dibutylamino group to the 6-carbonyl group would make the 6-carbonyl carbon weaker electrophilic than the 5-carbonyl carbon, so that the counter anions (Ph^-) preferentially attack the electrophilic 5-carbonyl carbon.

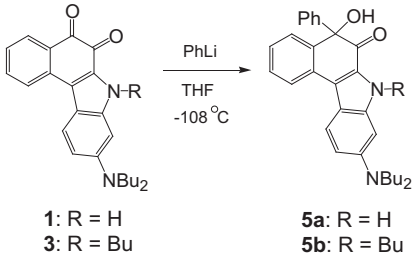

Scheme 3. Synthesis of quinols **5a** and **5b**.

2.2. Spectroscopic properties of 5a, 5b, and 6c in solution

The visible absorption and fluorescence spectral data of **5a**, **5b**, and **6c** in solution are summarized in Table 1. The fluorescence spectra of the three quinols were recorded by excitation at the wavelengths of the longest absorption maximum. As shown in Figure 1a, the three quinols exhibit two absorption maxima at around 340–385 nm and 430–440 nm in 1,4-dioxane, which are both red-shifted in the order of **6c** (340 and 430 nm) <**5a** (380 and 436 nm)≤**5b** (385 and 440 nm). On the other hand, the three

quinols exhibit a single fluorescence maximum at around 340–385 in 1,4-dioxane, which are also red-shifted in the order of **6c** (484 nm)≤**5a** (488 nm)≤**5b** (494 nm) as shown in Figure 1b. The fluorescence quantum yield (Φ) increases in the order of **5b** (0.35)≤**5a** (0.41)<**6c** (0.74) in 1,4-dioxane. The absorption maxima of the three quinols are nearly independent of solvent polarity, while the fluorescence maxima show a large red-shift on increasing the solvent polarity from 1,4-dioxane to ethanol. Therefore, the Stokes shift value in polar solvents becomes larger than that in non-polar solvents. Moreover, significant dependence of the fluorescence quantum yield on the solvent polarity was also observed: the Φ values of **5a**, **5b**, and **6c** are reduced to ca. 24% (0.41 in 1,4-dioxane to 0.10 in ethanol), 6% (0.35 in 1,4-dioxane to 0.02 in ethanol), and 20% (0.74 in 1,4-dioxane to 0.15 in ethanol), respectively, with increasing polarity from 1,4-dioxane to ethanol (Table 1).

Table 1
Absorption and fluorescence spectral data of **5a**, **5b**, and **6c** in solution

Quinol	Solvent	Absorption[a]	Fluorescence[b, c]	SS[d]
		λ_{max}/nm (ε_{max}/M^{-1} cm^{-1})	λ_{max}/nm (Φ_f)	$\Delta\lambda_{max}$/nm
5a	1,4-Dioxane	436(16,300), 380(13,300)	488 (0.41)	52
	Acetonitrile	444(18,800), 380(13,500)	535 (0.15)	91
	Ethanol	442(16,100), 382(13,200)	543 (0.10)	101
5b	1,4-Dioxane	440(30,200), 385(15,600)	494 (0.35)	54
	Acetonitrile	448(28,400), 389(14,800)	536 (0.16)	88
	Ethanol	444(29,400), 388(15,000)	540 (0.02)	96
6c	1,4-Dioxane	430(21,600), 340(9200)	484 (0.74)	54
	Acetonitrile	441(22,400), 343(10,000)	536 (0.30)	95
	Ethanol	441(22,800), 344(9500)	544 (0.15)	103

[a] 2.5×10^{-5} M.
[b] 2.5×10^{-6} M.
[c] Φ_f values were determined using 9,10-bisphenylethynylanthracene (Φ_f=0.84, λ_{ex}=440 nm) in benzene as a standard.
[d] Stokes shift value.

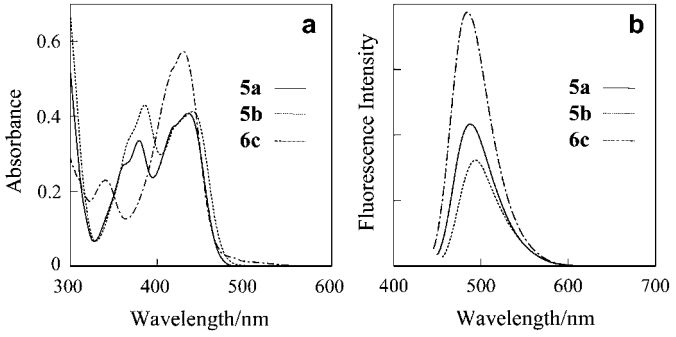

Figure 1. (a) Absorption and (b) fluorescence spectra of **5a**, **5b**, and **6c** in 1,4-dioxane.

2.3. Semi-empirical MO calculations (AM1, INDO/S)

The photophysical spectra of **5a**, **5b**, and **6c** were analyzed by using semi-empirical molecular orbital (MO) calculations. The molecular structures were optimized by using MOPAC/AM1 method[10], and then the INDO/S method[11] using the SCRF Onsager Model was used for spectroscopic calculations in 1,4-dioxane. The calculated absorption wavelengths and the transition character of the first and second absorption bands are collected in Table 2. The calculated absorption wavelengths and the oscillator strength values are relatively good compatible with the observed spectra in 1,4-dioxane, although the calculated absorption spectra are blue shifted. This deviation of the INDO/S calculations, giving high transition energies compared with the experimental values, has been generally observed.[12] The calculations show that the longest excitation bands for **5a**, **5b**, and **6c** are mainly assigned to the transition from the HOMO to the LUMO, where HOMO were mostly localized on the dibutylaminoindole moiety for **5a** and **5b** and the dibutylaminobenzofurano moiety for **6c**, and the LUMO were mostly localized on the naphthoquinol moiety for the three quinols. The values of the dipole moments in the ground states are 5.73 D for **5a**, 5.62 D for **5b**, and 7.33 D for **6c**. The differences between the dipole moments ($\Delta\mu$) of the first excited (HOMO→LUMO) and the ground states are 4.74 D for **5a**, 3.69 D for **5b**, and 6.53 D for **6c**. The changes in the calculated electron density accompanying the first electron excitation are shown in Figure 2, which reveal a strong migration of intramolecular charge transfer from dibutylaminoindole moiety or the dibutylaminobenzofurano moiety to the naphthoquinol moiety in the three quinols. These calculations indicate that the quinols **5a**, **5b**, and **6c** have similarly large dipole moments in their excited states, which explains well our finding that the three quinols show a large bathochromic shift of their fluorescence maxima in polar solvents and that the Stokes shift values for the three quinols in polar solvents are much larger than those in non-polar solvents.

Table 2
Calculated absorption spectra for **5a**, **5b**, and **6c**

Quinol	μ/D[a]	Absorption (calcd)		CI component[c]	$\Delta\mu$/D[d]
		λ_{max}/nm	f[b]		
5a	5.73	379	0.39	HOMO→LUMO (86%)	4.74
		340	0.17	HOMO-1→LUMO (60%)	3.16
5b	5.62	381	0.33	HOMO→LUMO (76%)	3.69
		344	0.17	HOMO-1→LUMO (62%)	3.66
6c	7.33	375	0.43	HOMO→LUMO (88%)	6.53
		325	0.18	HOMO-1→LUMO (51%)	1.74

[a] The values of the dipole moment in the ground state.
[b] Oscillator strength.
[c] The transition is shown by an arrow from one orbital to another, followed by its percentage CI (configuration interaction) component.
[d] The values of the difference in the dipole moment between the excited and the ground states.

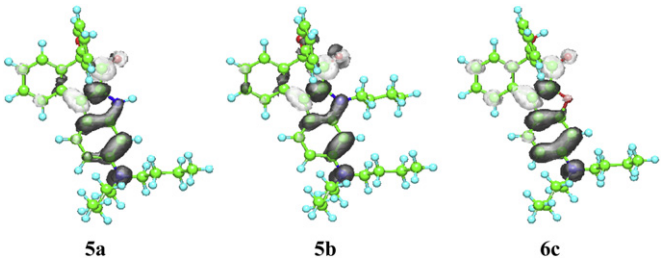

Figure 2. Calculated electron density changes accompanying the first electronic excitation of **5a**, **5b**, and **6c**. The black and white lobes signify the decrease and increase in electron density accompanying the electronic transition. Their areas indicate the magnitude of the electron density change.

2.4. Spectroscopic properties of 5a, 5b, and 6c in the solid state

Interesting results have been obtained from the photophysical properties of **5a**, **5b**, and **6c** in the solid state. Figure 3 shows that the optical properties of the three quinols are quite different between the solution and the solid state. The quinols **5a**, **5b**, and **6c** show yellowish-green in 1,4-dioxane, but orange, yellow, and yellowish-orange in the crystalline state, respectively. On the other hand, the three quinols exhibit bluish-green fluorescence emission in 1,4-dioxane, but the crystals of **5b** and **6c** exhibit green and greenish-yellow fluorescence emission, respectively. However, the

fluorescence of **5a** was strongly quenched in the solid state. In order to investigate the difference in the solid-state photophysical properties among the three quinols, we have measured the fluorescence excitation and emission spectra of the crystals. As shown in Figure 4, the wavelengths of the excitation and emission maxima of **5b** (λ_{ex}=485 nm, λ_{em}=518 nm) and **6c** (λ_{ex}=519 nm, λ_{em}=555 nm) are red-shifted by 45, 24 nm and 89, 71 nm compared with those in 1,4-dioxane, respectively, so that the red-shift values of **6c** from 1,4-dioxane to the solid state are larger than that of **5b**. The Φ values of **5b** and **6c** in the solid state are 0.07 and 0.03, respectively, which are smaller than those in 1,4-dioxane. The precise evaluation of the Φ value of **5a** was difficult because the fluorescence of **5a** was strongly quenched in the solid state. From a comparison of photophysical properties between solution and the solid states, it was found that the excitation and the emission maxima of **5a**, **5b**, and **6c** in the crystalline state are large red-shifted compared with those in 1,4-dioxane, and the Φ values of the three quinols in the crystalline state are much smaller that those in 1,4-dioxane.

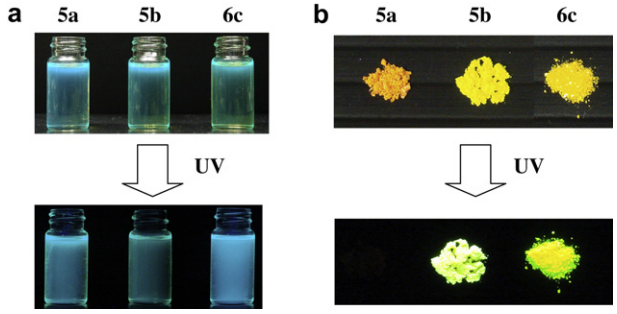

Figure 3. Fluorescence properties of **5a**, **5b**, and **6c** (a) in 1,4-dioxane and (b) in the solid state before and after UV irradiation.

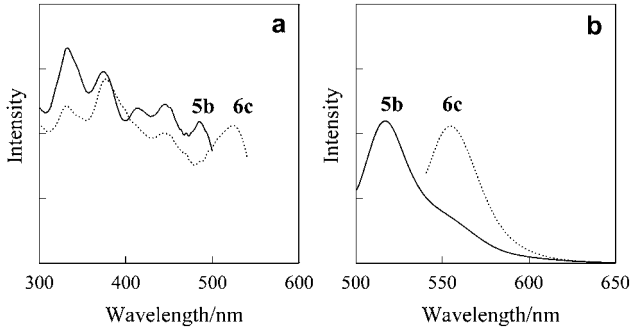

Figure 4. (a) Solid-state excitation and (b) emission spectra of the crystals of **5b** (λ_{ex}=485 nm, λ_{em}=518 nm, Φ=0.07) and **6c** (λ_{ex}=519 nm, λ_{em}=555 nm, Φ=0.03).

2.5. Relation between the solid-state fluorescence properties and X-ray crystal structures

In the previous paper, we have performed X-ray crystallographic analysis of **6c**.[6a] As shown in Figure 5a, the crystal of **6c** is built up by a centrosymmetric dimer unit, which is composed of a pair of quinol enantiomers: neighboring enantiomers are connected by two intermolecular hydrogen bonds between the hydroxyl and carbonyl oxygens through the hydroxyl proton (O(1)···O(2)* distance is 2.812 (4) Å). The intramolecular hydrogen bonding formation was also observed between the hydroxyl proton and the carbonyl oxygen in each quinol molecule (O(1)···O(2) distance is 2.740(2) Å). As shown in Figure 5b, there are five short interatomic contacts of less than 3.6 Å between the enantiomers and the π-overlappings were observed between the benzo[*b*]naphtho[1,2-*d*]furan planes. The interplanar distances between the benzo[*b*]naphtho[1,2-*d*]furan planes are ca. 3.58 Å, which suggests intermolecular π−π interactions between the fluorophores. Therefore, it has been concluded that the formation of intermolecular π−π interactions between the fluorophores is responsible for the large red-shift of the absorption and fluorescence maxima and a decrease in the solid-state fluorescence for **6c** from 1,4-dioxane to the solid state. Unfortunately, we could not obtain sufficient sizes of single crystals for **5b** to carry out the X-ray structural analysis, however, the relatively strong fluorescence intensity for the crystal of **5b** demonstrated that the N-butylation of carbazole moiety can effectively prevent the intermolecular π−π interactions between the fluorophores.

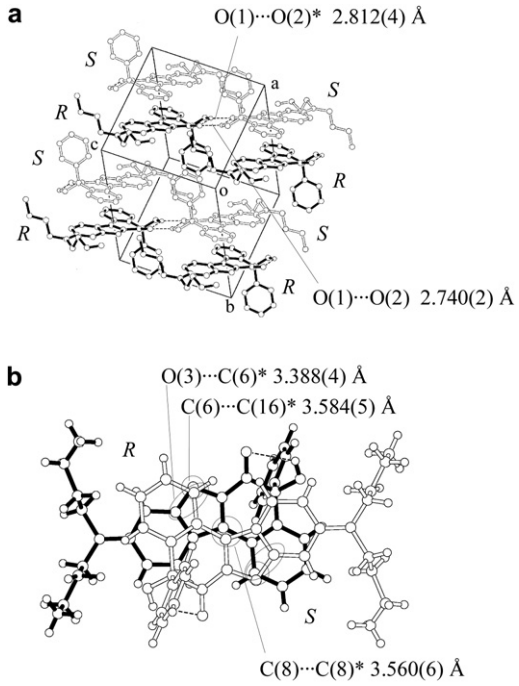

Figure 5. Crystal packing of **6c** (a) a stereoview of the molecular packing structure and (b) a top view of the pairs of fluorophores.

To elucidate the effects of the molecular packing structure on drastic solid-state fluorescence quenching for the crystals of **5a**, the X-ray crystal structure of **5a** has been determined. In the crystal of **5a**, there are no short π−π contacts of less than 3.60 Å between the neighboring fluorophores, which indicates the absence of the π−π interactions between the fluorophores (Fig. 6a). More interestingly, an one-dimensional chain is formed through three-type intermolecular hydrogen bonding between the equal enantiomers (Figs. 6b and c); the proton on carbazole nitrogen atom in the enantiomer is directing toward the carbonyl oxygen and the hydroxyl oxygen of another enantiomer to form the bifurcated intermolecular hydrogen bonding (N(1)H(2)···O(2)* angle=155(3)°, N(1)···O(2)* distance=2.897(4) Å; N(1)H(2)···O(1)* angle=126(1)°, N(1)···O(1)* distance=3.064(4) Å distance=2.800(4) Å), and the hydroxyl proton of the enantiomer is directing toward the carbonyl oxygen of another enantiomer (O(1)H(1)···O(2)** angle=145(4)°, O(1)···O(2)** distance=2.804(3) Å). Above results strongly reveal that the formation of a continuous intermolecular hydrogen bonding between the fluorophores is a principal factor of the drastic solid-state fluorescence quenching for the crystal of **5a**.

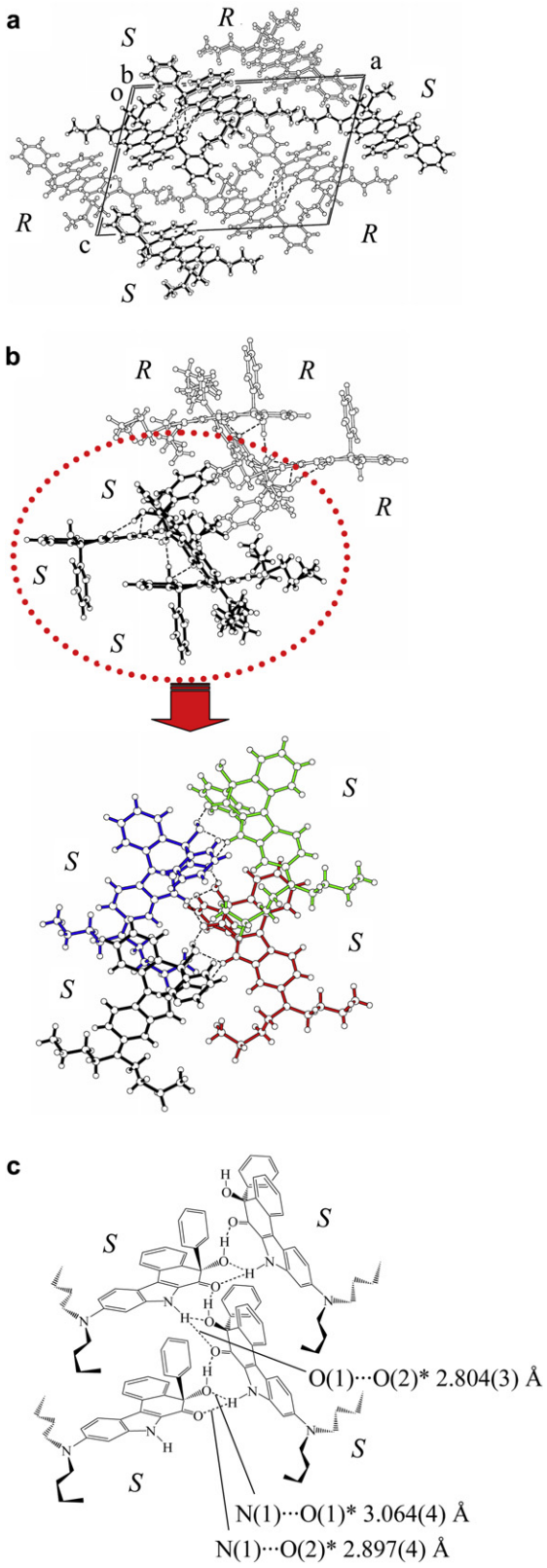

Figure 6. Crystal packing and hydrogen bonding pattern of **5a** (a) a stereoview of the molecular packing structure, (b) intermolecular hydrogen bonding between fluorophores and (c) a schematic structure.

3. Conclusion

To obtain variable information about the effect of molecular and crystal structures on the solid-state fluorescence properties, the three heterocyclic quinol-type fluorophores with benzo[*c*]carbazol-6-one skeleton or benzo[*b*]naphtho[1,2-*d*]furan-6-one skeleton have been derived from the corresponding *o*-quinones and their photophysical properties have been investigated in solution and in the solid state. The three quinols exhibit a moderate fluorescence intensity in 1,4-dioxane. However, the fluorescence of **5a** with benzo[*c*]carbazol-6-one skeleton was strongly quenched in the solid state. The X-ray crystal structure of **5a** demonstrated that the formation of a continuous intermolecular hydrogen bonding between the fluorophores is a principal factor of a drastic solid-state fluorescence quenching for the crystal of **5a**. Thus, new valuable information concerning the effect of molecular and crystal structures on the solid-state fluorescence of organic fluorescent dyes has been obtained.

4. Experimental

4.1. General

Elemental analyses were measured with a Perkin–Elmer 2400 II CHN analyzer. IR spectra were recorded on a JASCO FT/IR-5300 spectrophotometer for samples in KBr pellet form. Single-crystal X-ray diffraction was performed on Rigaku AFC7S diffractometer. Absorption spectra were observed with a JASCO U-best30 spectrophotometer and fluorescence spectra were measured with a JASCO FP-777 spectrophotometer. The fluorescence quantum yields (Φ) in benzene were determined using 9,10-bisphenylethynylanthracene (Φ=0.84, λ_{ex}=440 nm)[13] in benzene as the standard. For the measurement of the solid-state fluorescence excitation and emission spectra of the crystals, Jasco FP-1060 attachment was used. The solid-state fluorescence quantum yields (Φ) were determined by a Hamamatsu C9920-01 equipped with CCD by using a calibrated integrating sphere system (λ_{ex}=485 nm for **5b** and λ_{ex}=519 nm for **6c**). ^{1}H NMR spectra were recorded on a JNM-LA-400 (400 MHz) FT NMR spectrometer with tetramethylsilane (TMS) as an internal standard.

4.2. Synthesis

*4.2.1. 9-Dibutylamino-7H-benzo[c]carbazole-5,6-dione (**1**) and 4-(3-dibutylamino-phenylamino)-[1,2]naphthoquinone (**2**).* To a solution of sodium 1,2-naphthoquinone-4-sulfonate (10.38 g, 40 mmol) and $Ni(OCOCH_3)_2 \cdot 4H_2O$ (9.93 g, 40 mmol) in acetic acid aqueous solution (80%, 250 ml) was add *m*-amino-*N*,*N*-dibutylaniline (8.8 g, 40 mmol) with stirring at room temperature. After further stirring for 12 h, the reaction mixture was poured into water. The resulting precipitate was filtered, washed with water and dried. The residue was chromatographed on silica gel (*n*-hexane/ethyl acetate=2:1 as eluent) to give **1** (0.8 g, yield 5%) as a purple powder and **2** (5.3 g, yield 35%) as a red powder.

Compound **1**: mp 221–222 °C; ^{1}H NMR (400 MHz, DMSO-d_6, TMS) δ=0.93 (t, J=7.3 Hz, 6H), 1.32–1.37 (m, 4H), 1.52–1.57 (m, 4H), 3.22–3.51 (m, 4H) (overlapping peak of dissolved water in DMSO-d_6), 6.39 (s, 1H), 6.82 (d, J=9.5 Hz, 1H), 7.30 (t, J=7.6 Hz, 1H), 7.62 (t, J=7.8 Hz, 1H), 7.81 (d, J=9.5 Hz, 1H), 8.00–8.04 (m, 2H), 11.7 (s, 1H, –NH); IR (KBr): ν=3312, 1685, 1636 cm^{-1}; MS (ESI, m/z) 375 $[M+H]^+$

Compound **2**: mp 204–205 °C; ^{1}H NMR (400 MHz, DMSO-d_6, TMS) δ=0.90 (t, J=7.3 Hz, 6H), 1.25–1.35 (m, 4H), 1.46–1.54 (m, 4H), 3.20–3.50 (m, 4H) (overlapping peak of dissolved water in DMSO-d_6), 5.78 (s, 1H), 6.52–6.57 (m, 3H), 7.22 (t, J=7.8 Hz, 1H), 7.72 (t, J=7.6 Hz, 1H), 7.85 (t, J=7.8 Hz, 1H), 8.03 (d, J=8.0 Hz, 1H), 8.31

(d, J=8.0 Hz, 1H), 9.76 (br, 1H, −NH); IR (KBr): ν=3315, 1584 cm^{-1}; MS (ESI, m/z) 377 $[M+H]^+$

*4.2.2. 7-Butyl-9-dibutylamino-7H-benzo[c]carbazole-5,6-dione (**3**) and 11-butyl-9-dibutylamino-11H-benzo[a]carbazole-5,6-dione (**4**).* To a solution of sodium 1,2-naphthoquinone-4-sulfonate (0.5 g, 1.92 mmol) and $CuCl_2$ (0.26 g, 1.92 mmol) in DMF (10 ml) was add *m*-butylamino-*N*,*N*-dibutylaniline (0.53 g, 1.92 mmol) with stirring at 80 °C. After further stirring for 2 h, the reaction mixture was poured into water. The resulting precipitate was filtered, washed with water, and dried. The residue was chromatographed on silica gel (CH_2Cl_2 as eluent) to give **3** (0.32 g, yield 39%) as a black powder and **4** (0.11 g, yield 13%) as a brown powder.

Compound **3**: mp 169–170 °C; ^{1}H NMR (400 MHz, $CDCl_3$, TMS) δ=0.94–1.02 (m, 9H), 1.36–1.46 (m, 6H), 1.62–1.70 (m, 4H), 1.71–1.81 (m, 2H), 3.40 (t, J=8.3 Hz, 4H), 4.47 (t, J=9.6 Hz, 2H), 6.20 (d, J=2.0 Hz, 1H), 6.78 (dd, J=2.0 and 9.3 Hz, 1H), 7.23 (t, J=7.9 Hz, 1H), 7.52 (t, J=7.7 Hz, 1H), 7.88–7.93 (m, 2H), 7.99 (dd, J=1.5 and 7.6 Hz, 1H); IR (KBr): ν=1690, 1637 cm^{-1}; MS (ESI, m/z) 431 $[M+H]^+$

Compound **4**: mp 87–89 °C; ^{1}H NMR (400 MHz, $CDCl_3$, TMS) δ=0.91–1.00 (m, 9H), 1.25–1.44 (m, 6H), 1.59–1.67 (m, 4H), 1.78–1.87 (m, 2H), 3.35 (t, J=7.6 Hz, 4H), 4.15 (t, J=7.1 Hz, 2H), 6.21 (d, J=2.0 Hz, 1H), 6.68 (dd, J=2.0 and 9.0 Hz, 1H), 6.92 (t, J=7.3 Hz, 1H), 6.99 (d, J=7.1 Hz, 1H), 7.13 (t, J=6.8 Hz, 1H), 7.20 (d, J=7.1 Hz, 1H), 7.44 (d, J=9.0 Hz, 1H); IR (KBr): ν=1681 cm^{-1}.

*4.2.3. General synthetic procedure for the quinols **5a** or **5b** by the reaction of quinones **1** or **3** with phenyllithium reagent.* To a THF solution of quinone **1** (or **3**) under an argon atmosphere was added ethereal solution of phenyllithium at −108 °C over 15 min. During the course of addition, the red solution turned to a reddish brown solution. After stirring for 15 min at room temperature, the reaction was quenched with saturated NH_4Cl solution. The solvent was evaporated and the residue was extracted with CH_2Cl_2. The organic extract was washed with water. The CH_2Cl_2 extract was evaporated and the residue was chromatographed on silica gel (CH_2Cl_2/ethyl acetate=10:1 as eluent) to give **5a** or **5b**.

*4.2.3.1. 9-Dibutylamino-5-hydroxy-5-phenyl-5,7-dihydro-benzo[c]carbazol-6-one (**5a**).* Yield 21%, an orange powder; mp 209–215 °C; ^{1}H NMR (400 MHz, $CDCl_3$, TMS) δ=0.98 (t, J=7.4 Hz, 6H), 1.35–1.45 (m, 4H), 1.60–1.67 (m, 4H), 3.37 (t, J=7.8 Hz, 4H), 4.45 (s, 1H, −OH), 6.43 (d, J=2.2 Hz, 1H), 6.82 (dd, J=2.2 and 9.2 Hz, 1H), 7.13–7.43 (m, 7H), 7.56 (dd, J=1.2 and 7.8 Hz, 1H), 8.06–8.14 (m, 2H), 8.64 (br, 1H, −NH); IR (KBr): ν=3418, 3258, 1633 cm^{-1}. Anal. Calcd (%) for $C_{30}H_{32}N_2O_2$: C 79.61, H 7.13, N 6.19; found: C 79.96, H 7.18, N 6.20.

*4.2.3.2. 7-Butyl-9-dibutylamino-5-hydroxy-5-phenyl-5,7-dihydro-benzo[c]carbazol-6-one (**5b**).* Yield 12%, a yellow powder; mp 118–120 °C; ^{1}H NMR (400 MHz, $CDCl_3$, TMS) δ=0.73 (t, J=7.3 Hz, 3H), 0.97–1.10 (m, 8H), 1.36–1.45 (m, 4H), 1.56–1.69 (m, 6H), 3.39 (t, J=7.8 Hz, 4H), 4.42–4.29 (m, 1H), 4.44–4.51 (m, 1H), 4.82 (s, 1H, −OH), 6.30 (d, J=2.2 Hz, 1H), 6.82 (dd, J=2.2 and 9.3 Hz, 1H), 7.12–7.41 (m, 7H), 7.58 (dd, J=1.5 and 7.8 Hz, 1H), 8.09–8.15 (m, 2H); IR (KBr): ν=3440, 1637 cm^{-1}; MS (ESI, m/z) 509 $[M+H]^+$

4.3. Computational methods

All calculations were performed on FUJITSU FMV-ME4/657. The semi-empirical calculations were carried out with the WinMOPAC Ver. 3.9 package (Fujitsu, Chiba, Japan). Geometry calculations in the ground state were carried out using the AM1 method.[10] All geometries were completely optimized (keyword PRECISE) by the eigenvactor following routine (keyword EF). Experimental absorption spectra of the compounds were studied with the semi-empirical method INDO/S (intermediate neglect of differential overlap/spectroscopic)[11] using the SCRF Onsager Model. All INDO/S calculations were performed using single excitation full SCF/CI (self-consistent field/configuration interaction), which includes the configuration with one electron excited from any occupied orbital to any unoccupied orbital, 225 configurations were considered for the configuration interaction [keyword CI (15 15)].

4.4. X-ray crystallographic studies

The data sets were collected at 23±1 °C on a Rigaku AFC7S four-circle diffractometer by $2\theta-\omega$ scan technique, and using graphite-monochromated Mo Kα (λ=0.71069 Å) radiation at 50 kV and 30 mA. In all case, the data were corrected for Lorentz and polarization effects. A correction for secondary extinction was supplied. The reflection intensities were monitored by three standard reflections for every 150 reflections. An empirical absorption correction based on azimuthal scans of several reflections was applied. All calculations were performed using the teXsan[14] crystallographic software package of Molecular Structure Corporation.

*4.4.1. Crystal structure determination of compound **5a**.* Crystal of **5a** was recrystallized from dichloromethane/*n*-hexane as orange prism, air stable. The one selected had approximate dimensions 0.25×0.25×0.35 mm. The transmission factors ranged from 0.98 to 1.00. The crystal structure was solved by direct methods using SIR 92.[15] The structures were expanded using Fourier techniques.[16] The non-hydrogen atoms were refined anisotropically. Some hydrogen atoms were refined isotropically, the rest were fixed geometrically and not refined. Crystal data for **5a**: $C_{30}H_{32}N_2O_2$, M=452.59, monoclinic, a=22.388(3), b=7.749(1), c=14.871(2) Å, β=106.501 (8)°, U=2473.8(5) $Å^3$, ρ_{calcd}=1.215 gcm^{-3}, T=297 K, space group $P2_1/n$ (no.14), Z=4, μ(Mo Kα)=0.76 cm^{-1}, 6248 reflections measured, 5815 unique (R_{int}=0.016), which were used in all calculations. The final R indices [$I>2\sigma(I)$], R_1=0.063, $wR(F^2)$=0.174. Crystallographic data (excluding structure factors) has been deposited with Cambridge Crystallographic Data Centre as supplementary publication number CCDC 783289. These data can be obtained free of charge from The Cambridge Crystallographic Data Centre via www.ccdc.cam.au.uk/data_request/cif.

Acknowledgements

This work was supported in part by a Grant-in-Aid for Scientific Research (C) (21550181) from the Japan Society for the Promotion of Science.

Supplementary data

Supplementary data associated with this article can be found in the online version at doi:10.1016/j.tet.2010.08.026.

References and notes

1. (a) Langhals, H.; Potrawa, T.; Nöth, H.; Linti, G. *Angew. Chem., Int. Ed. Engl.* **1989**, *28*, 478; (b) Langhals, H.; Ismael, R.; Yürük, O. *Tetrahedron* **2001**, *56*, 5435; (c) de Halleux, V.; Calbert, J.-P.; Brocorens, P.; Cornil, J.; Declercq, J.-P.; Brédas, J.-L.; Geerts, Y. *Adv. Funct. Mater.* **2004**, *14*, 649; (d) Yeh, H.-C.; Wu, W.-C.; Wen, Y.-S.; Dai, D.-C.; Wang, J.-K.; Chen, C.-T. *J. Org. Chem.* **2004**, *69*, 6455; (e) Mizobe, Y.; Tohnai, N.; Miyata, M.; Hasegawa, Y. *Chem. Commun.* **2005**, 1839; (f) Vayá, I.; Jiménez, M. C.; Miranda, M. *Tetrahedron: Asymmetry* **2005**, *16*, 2167; (g) Zhao, C.-H.; Wakamiya, A.; Inukai, Y.; Yamaguchi, S. *J. Am. Chem. Soc.* **2006**, *128*, 15934; (h) Iida, A.; Yamaguchi, S. *Chem. Commun.* **2009**, 3002; (i) Mizobe, Y.; Hinoue, T.; Yamamoto, A.; Hisaki, I.; Miyata, M.; Hasegawa, Y.; Tohnai, N. *Chem.—Eur. J.* **2009**, *15*, 8175.
2. (a) Tang, C. W.; VansSlyke, S. A. *Appl. Phys. Lett.* **1987**, *51*, 913; (b) Tang, C. W.; VansSlyke, S. A.; Chen, C. H. *J. Appl. Phys.* **1989**, *65*, 3610; (c) Schi, J.; Tang, C. W. *Appl. Phys. Lett.* **1997**, *70*, 1665; (d) Kraft, A.; Grimsdale, A. C.; Holmes, A. B. *Angew. Chem., Int. Ed.* **1998**, *37*, 402; (e) Mitschke, U.; Bäuerle, P. *J. Mater. Chem.*

2000, *10*, 1471; (f) Wong, K.-C.; Chien, Y.-Y.; Chen, R.-T.; Wang, C.-F.; Liu, Y.-T.; Chiang, H.-H.; Hsieh, P.-Y.; Wu, C.-C.; Chou, C. H.; Su, Y. O.; Lee, G.-H.; Peng, S.-M. *J. Am. Chem. Soc.* **2002**, *124*, 11576; (g) Tonzola, C. J.; Alam, M. M.; Kaminsky, W. K.; Jenekhe, S. A. *J. Am. Chem. Soc.* **2003**, *125*, 13548; (h) Yeh, H.-C.; Chan, L.-H.; Wu, W.-C.; Chen, C.-T. *J. Mater. Chem.* **2004**, *14*, 1293; (i) Chen, C.-T. *Chem. Mater.* **2004**, *16*, 4389; (j) Chiang, C.-L.; Wu, M.-F.; Dai, D.-C.; Wen, Y.-S.; Wang, J.-K.; Chen, C.-T. *Adv. Funct. Mater.* **2005**, *15*, 231.

3. (a) Yoshida, K.; Yamazaki, J.; Tagashira, Y.; Watanabe, S. *Chem. Lett.* **1996**, 9; (b) Yoshida, K.; Tachikawa, T.; Yamasaki, J.; Watanabe, S.; Tokita, S. *Chem. Lett.* **1996**, 1027; (c) Yoshida, K.; Miyazaki, H.; Miura, Y.; Ooyama, Y.; Watanabe, S. *Chem. Lett.* **1999**, 837; (d) Yoshida, K.; Ooyama, Y.; Tanikawa, S.; Watanabe, S. *Chem. Lett.* **2000**, 714; (e) Yoshida, K.; Ooyama, Y.; Tanikawa, S.; Watanabe, S. *J. Chem. Soc., Perkin Trans. 2* **2002**, 708; (f) Ooyama, Y.; Yoshida, K. *New J. Chem.* **2005**, *29*, 1204; (g) Ooyama, Y.; Kagawa, Y.; Fukuoka, H.; Ito, G.; Harima, Y. *Eur. J. Org. Chem.* **2009**, *31*, 5321.
4. (a) Yoshida, K.; Ooyama, Y.; Miyazaki, H.; Watanabe, S. *J. Chem. Soc., Perkin Trans. 2* **2002**, 700; (b) Ooyama, Y.; Nakamura, T.; Yoshida, K. *New J. Chem.* **2005**, *29*, 447; (c) Horiguchi, E.; Matsumoto, S.; Funabiki, K.; Matsui, M. *Bull. Chem. Soc. Jpn.* **2005**, *78*, 1167; (d) Mizukami, S.; Houjou, H.; Sugaya, K.; Koyama, E.; Tokuhisa, H.; Sasaki, T.; Kanesato, M. *Chem. Mater.* **2005**, *17*, 50.
5. (a) Davis, R.; Abraham, S.; Rath, N. P.; Das, S. *New J. Chem.* **2004**, *28*, 1368; (b) Horiguchi, E.; Matsumoto, S.; Funabiki, K.; Matsui, M. *Bull. Chem. Soc. Jpn.* **2006**, *79*, 799; (c) Chung, H. W.; Yang, H.; Singh, B.; Moon, H.; An, B.-K.; Lee, S. Y.; Park, S. Y. *J. Mater. Chem.* **2009**, *19*, 5920.
6. (a) Ooyama, Y.; Okamoto, T.; Yamaguchi, T.; Suzuki, T.; Hayashi, A.; Yoshida, K. *Chem.—Eur. J.* **2006**, 7827; (b) Ooyama, Y.; Yoshikawa, S.; Watanabe, S.; Yoshida, K. *Org. Biomol. Chem.* **2006**, *4*, 3406; (c) Ooyama, Y.; Yoshikawa, S.; Watanabe, S.; Yoshida, K. *Org. Biomol. Chem.* **2007**, *5*, 1260; (d) Ooyama, Y.; Kagawa, Y.; Harima, Y. *Eur. J. Org. Chem.* **2007**, 3613; (e) Ooyama, Y.; Hayashi, A.; Okamoto, T.; Egawa, H.; Mamura, T.; Yoshida, K. *Eur. J. Org. Chem.* **2008**, 3085.
7. Ozdemir, T.; Atilgan, S.; Kutuk, I.; Yildirm, L. T.; Tulek, A.; Bayindir, M.; Akkaya, E. U. *Org. Lett.* **2009**, *11*, 2105.
8. (a) Luo, J.; Xie, Z.; Lam, J. W. Y.; Cheng, L.; Chen, H.; Qiu, C.; Kwok, H. S.; Zhan, X.; Liu, Y.; Zhu, D.; Tang, B. Z. *Chem. Commun.* **2001**, 1740; (b) Tang, B. Z.; Zhan, X.; Yu, G.; Lee, P. P. S.; Liu, Y.; Zhu, D. *J. Mater. Chem.* **2001**, *11*, 2974; (c) Dong, Y.; Lam, J. W. Y.; Qin, A.; Li, Z.; Sun, J.; Sung, H. H.-Y.; Williams, I. D.; Tang, B. Z. *Chem. Commun.* **2007**, 40; (d) Hong, Y.; Lam, J. W. Y.; Tang, B. Z. *Chem. Commun.* **2009**, 4332.
9. (a) Fischer, A.; Henderson, G. N. *Tetrahedron Lett.* **1980**, *21*, 701; (b) Fischer, A.; Henderson, G. N. *Tetrahedron Lett.* **1983**, *24*, 131; (c) Mckinley, J.; Aponick, A.; Raber, J. C.; Fritz, C.; Montgomery, D.; Wigal, C. T. *J. Org. Chem.* **1997**, *62*, 4874.
10. Dewar, M. J. S.; Zoebisch, E. G.; Healy, E. F.; Stewart, J. J. P. *J. Am. Chem. Soc.* **1985**, *107*, 3902.
11. (a) Ridley, J. E.; Zerner, M. C. *Theor. Chim. Acta* **1973**, *32*, 111; (b) Ridley, J. E.; Zerner, M. C. *Theor. Chim. Acta* **1976**, *42*, 223; (c) Bacon, A. D.; Zerner, M. C. *Theor. Chim. Acta* **1979**, *53*, 21.
12. (a) Adachi, M.; Murata, Y.; Nakamura, S. *J. Org. Chem.* **1993**, *58*, 5238; (b) Fabian, W. M. F.; Schuppler, S.; Wolfbeis, O. S. *J. Chem. Soc., Perkin Trans. 2* **1996**, 853.
13. Heller, C. A.; Henry, R. A.; Mclaughlin, B. A.; Bills, D. E. *J. Chem. Eng. Data* **1974**, *19*, 214.
14. teXsan: *Crystal Structure Analysis Package*; Molecular Structure Corporation: The Woodlands, TX, 1985 and 1992.
15. Altomare, A.; Burla, M. C.; Camalli, M.; Cascarano, M.; Giacovazzo, C.; Guagliardi, A.; Polidori, G. *J. Appl. Crystallogr.* **1994**, *27*, 435.
16. DIRDIF94. Beurskens, P. T.; Admiraal, G.; Beurskens, G.; Bosman, W. P.; de Gelder, R.; Israel, R.; Smits, J. M. M. *The DIRIF94 program system, Technical Report of the Crystallography Laboratory*; University of Nijmegen: The Netherlands, 1994.